CANCER BIOTHERAPY & RADIOPHARMACEUTICALS
Volume 18, Number 2, 2003

Three-Dimensional Dose Model for the Comparison of ^{177}Lu-HuCC49ΔCH2 and ^{177}Lu-HuCC49 Radioimunotherapy in Mice Bearing Intraperitoneal Xenografts

Peter L. Roberson, Ph.D.,[1] Shigeru Yokoyama, Ph.D.,[1] Buck E. Rogers, Ph.D.,[2] and Donald J. Buchsbaum, Ph.D.[2]
[1]University of Michigan, Ann Arbor, MI 48109; [2]University of Alabama at Birmingham, Birmingham, AL 35294

ABSTRACT

Uptake and dose distributions in peritoneal LS174T colon tumor xenografts were compared for a humanized construct of the CC49 (HuCC49) high-affinity anti-TAG-72 monoclonal antibody and a construct with the CH2 region deleted (HuCC49ΔCH2), both labeled with ^{177}Lu using a PA-DOTA bifunctional chelating agent and injected in the peritoneum. Tumors were resected and serially sectioned at 1 h, 4 h, 24 h, and 48 h postinjection. Between 5 and 24 (average 16) sections were retained per tumor for autoradiography. The typical section interval was 340 μm and thickness was 16 μm. Tumor sections were air dried and placed on film and/or phosphor screen. Section images were digitized at 100 μm resolution electronically (phosphor screen) or by laser densitometer (film). Section images were used to generate tumor surface descriptions and activity distributions by reconstructing the activity densities in three dimensions. Three-dimensional dose-rate calculations, performed using a point kernel for ^{177}Lu, were used to prepare radial histograms describing the variation in dose rate as a function of distance from the tumor center to surface. At early times postinjection, the ^{177}Lu-HuCC49ΔCH2 antibody displayed higher dose rates near the tumor surface compared to the ^{177}Lu-HuCC49 antibody. At 24 h postinjection, dose rate distributions appeared similar for both antibodies and more uniform than at earlier times. The ^{177}Lu-HuCC49ΔCH2 antibody indicated improved uniformity at 48 h postinjection. Cell survival calculations based on the three-dimensional dose rate distributions favored ^{177}Lu-HuCC49ΔCH2 for equal injection activities. However the most significant effect was the greater injected dose tolerated for the ^{177}Lu-HuCC49ΔCH2 antibody based on equivalent estimated bone marrow dose.

Key Words: dosimetry, radioimmunotherapy, ^{177}Lu, effective dose, autoradiography

INTRODUCTION

Changes in the delivery systems and isotopes used for radioimmunotherapy of cancer have a significant impact on outcome. Predicted and actual therapy results can be better understood using detailed dosimetric studies. It is hoped that future therapy regimen designs can benefit from improved dosimetric analyses.

Limitations to the use of radioimmunotherapy for the treatment of cancer have included the human anti-murine antibody (HAMA) response due to the use of murine mAbs, myelotoxicity due to slow clearance of the radiolabeled mAbs from serum, and slow and nonuniform uptake of mAbs

Corresponding author: Peter L. Roberson, Ph.D., Department of Radiation Oncology, University of Michigan, UH-B2C490, 1500 E. Medical Center Dr., Ann Arbor, MI 48109, Tel: 734-936-4309, Fax: 734-936-7859, E-mail: roberpl@umich.edu

in tumor. A greater choice of radioisotopes (^{177}Lu, $^{64/67}$Cu, $^{186/188}$Re, ^{90}Y) followed the development of improved bifunctional chelating agents capable of forming highly stable complexes with radiometals.[1] These isotopes (except ^{90}Y) have potentially favorable beta and photon characteristics and lack the *in vivo* deiodination of ^{131}I. The HAMA response in patients has been mitigated through genetically engineered mAbs, particularly humanized mAbs with only the antigen-binding complementary-determining region from the native murine mAbs.[2,3] However, the humanized mAbs may produce increased myelotoxicity due to even slower clearance from serum.

Myelotoxicity can be decreased by increasing the serum clearance of mAbs through decreased molecular size. Decrease in molecular size has been achieved through the use of mAb fragments and genetically engineered single-chain variable regions. Drawbacks include increased radiation dose to kidneys, lower antigen affinity, and decreased radiation dose to the tumor due to lower binding rates and increased clearance from tumor. A potential advantage is increased uptake uniformity in tumor due to improved mobility. Another option to reduce molecular size is to delete the CH1 or CH2 domain of the constant region of the mAb, which is replaced with a peptide linker. It has been postulated that more rapid serum clearance occurs not only because of decreased molecular size, but also because of removal of the glycosylation site in the CH2 region, which may facilitate receptor-mediated clearance through the liver.[4] The use of a humanized mAb with CH2 region deleted may improve therapeutic results through lower immunogenicity, rapid blood clearance, and comparable tumor localization.

CC49 is a second-generation murine mAb reactive with the TAG-72 antigen, present on a variety of adenocarcinomas. It has a higher binding affinity for TAG-72 compared to its precursor mAb, B72.3, and has been radiolabeled with ^{131}I, ^{90}Y, and ^{177}Lu.[5–7] Lutetium-177 has a 6.7-day half-life, a maximum beta emission of 497 keV and relatively low branching ratios for gamma emissions, useful for imaging. The lower energy beta spectrum of ^{177}Lu, compared to ^{131}I, increases dose rates at tumor surface regions, but provides less radiation cross-talk in more central, low-uptake regions.[8] However, the expected improved uniformity of uptake for the CH2-deleted mAb may favor the less penetrating beta spectrum, particularly in tumor surface regions.

We report on comparative dosimetry studies for peritoneal LS174T colon tumor xenografts, receiving ^{177}Lu-PA-DOTA-HuCC49 or ^{177}Lu-PA-DOTA-HuCC49ΔCH2 mAbs by intraperitoneal injection. The dosimetric comparison will focus on the changes in three-dimensional (3D) dose-rate distributions with time postinjection.

MATERIALS AND METHODS

Tumor Model

Four- to five-week-old athymic nude mice (National Cancer Institute Frederick Research Laboratory, Frederick, MD), implanted i.p. with 5 x 10^7 LS174T cells, received an i.p. injection of ^{177}Lu-PA-DOTA-HuCC49 or ^{177}Lu-PA-DOTA-HuCC49ΔCH2 (30 μCi to 300 μCi) 8 days post tumor-cell injection. Additional experimental details and biodistribution data are presented elsewhere.[9]

Tumors were resected, frozen and serially sectioned at 1 h, 4 h, 24 h, and 48 h postinjection with ^{177}Lu-PA-DOTA-HuCC49 or ^{177}Lu-PA-DOTA-HuCC49ΔCH2 mAbs. Between 5 and 24 (average 16) sections were retained per tumor for autoradiography. The typical interval between sections was 340 μm. Section thickness was 16 μm. Tumor sections were air dried and placed on film (Super RX 20.3 x 25.4 cm, FujiFilm, Stamford, CT) and/or phosphor screen (BAS-MS Imaging Plates 20 x 25 cm with BAS-1800 scanner, FujiFIlm, Stamford, CT) for autoradiography. Section images from film were digitized at 100 μm resolution using a laser densitometer (Lumysis, Sunnyvale, CA). Phosphor imager pixel resolution was set to 100 μm. Film and phosphor screen responses were measured using gel samples with known activity density, which were sectioned and imaged along with the tumor sections.

Activity Density Distributions

Three-dimensional activity and dose-rate distributions were generated using image-based treatment planning software written by the University of Michigan (UMPLAN) together with adjunct software designed specifically to work with UMPLAN. Serial sections for each tumor were imaged together in approximate alignment. The positions of the electronic section images were translated and rotated to produce optimum alignment. Optimum alignment was determined based

on external contour and internal structure matching via operator judgment and independent review. Spaces between section images were determined from gaps skipped between sections. Tumor surface descriptions were generated by autocontouring of the digitized section images and using 3D surface-rendering software within UMPLAN. The first and last contours were capped corresponding to approximately half a sectioning interval. Surface contour generation criteria were checked by comparing the results to a sampling of optically scanned images of section slides. The reconstructed tumor volumes were compared for consistency to the tumor masses measured before sectioning. Section images, image intensity calibration curves, and alignment parameters were used to create 3D activity density distributions. A linear interpolation of activity density information between sections filled the 3D activity density matrix. The activity density distributions were superimposed on section images to check proper alignment and approximate activity density magnitudes.

Three-dimensional dose-rate distributions were calculated using a point kernel for ^{177}Lu.[10] Voxel kernels were calculated by distributing 64 point kernels in the voxel volume. The voxel kernel was folded with the activity density matrix using Fast Fourier analysis. Most tumor matrices were summed to a $(0.2\ \text{mm})^3$ cubic voxel for the dose rate calculation due to limitations on matrix size imposed by UMPLAN (128 x 128 x 128). Dose calculations for the remainder (smaller tumors) were performed using the original $(0.1\ \text{mm})^3$ voxel. The results of dose-rate calculations were superimposed on the section images as a check on alignment and approximate dose-rate magnitudes. Detailed procedures have appeared elsewhere.[11,12]

Dosimetry Model

The dose-rate information was used to prepare radial histograms describing the variation in dose rate as a function of fractional distance from the tumor center of mass to the tumor surface. The histograms represent dose-rate distributions for 30 radial increments. This procedure isolated surface compared to central tumor uptake characteristics. Some tumors appeared as two or three separate nodules rather than one solitary nodule. These were treated as separate tumors, or were discarded as unusually small ancillary nodules. Radial histograms were averaged to produce dose-rate descriptions representative of average behavior at each time point postinjection. Histograms were normalized to the average dose rate values calculated from the tumor uptake measurements (Fig. 1b). The range of dose rates observed was preserved in the average, whether for a smaller than average tumor or a larger than average tumor.

The radially dependent histograms and the average dose rates derived from the uptake curves together represented the spatially and temporally varying dose-rate description. For times between measured uptake distributions, linear interpolation of the dose-rate distributions was performed. The averaged dose-rate data represented an idealized history of a representative tumor.

Tumor dose rates were summed over time to yield cumulative dose distributions. Each radial increment was summed with like radial increments from the other averaged histograms. In each radial increment, dose rates were summed assuming the approximation of maximum heterogeneity. This is equivalent to assuming that well and poorly vascularized regions remained distinct during the time course of the idealized tumor. Detailed procedures have appeared elsewhere.[12,13]

Effective Dose

Effective dose calculations were performed using the dosimetry model. The effective dose was defined as the uniform dose required for an equivalent minimum fractional cell survival (S), assuming a linear (α) dose response:

$$Deff = -1/\alpha[\ln(S)]_{\min}$$

For a temporally and spatially varying dose distribution:

$$S(t) = 1/V \int_V \exp\left(-\alpha \int_0^t R(\vec{r},t')dt' RE(\vec{r},t)\right)d^3r$$

where RE is the relative effectiveness factor assuming the linear quadratic model[14,15] and V is the tumor volume.

Cell survival calculations also assumed an approximate relative cell proliferation rate based on observed fractional necrotic volumes of ~30%. Fractional volume functions for necrotic, hypoxic, and oxygenated cells were derived as a function of vessel spacing. The hypoxic and necrotic partial volumes were estimated by folding the fractional volume function with the vascular density function. The normalization was adjusted to yield a 0.3 fractional necrotic volume,

resulting in a net fractional hypoxic volume of 0.1. The fraction of oxygenated cells increased from the interior (~0.5) to the surface (~0.7) with the corresponding decrease in necrotic cells. Oxygenated cells were assumed to proliferate while hypoxic cells remained dormant. Cell survival equations were:

$$S(t) = 1/V \int_V [S_O(\vec{r},t)F_O(\vec{r}) + S_H(\vec{r},t)F_H(\vec{r})]d^3r$$

where

$$S_O(\vec{r},t) = \exp\left(-\alpha_O \int_0^t R(\vec{r},t')dt' RE_O(\vec{r},t) + \lambda t\right)$$

$$S_H(\vec{r},t) = \exp\left(-\alpha_H \int_0^t R(\vec{r},t')dt' RE_H(\vec{r},t)\right)$$

and the subscripts represent oxygenated and hypoxic components, necrotic cells do not contribute to S, F_O and F_H are the radially dependent fractional volumes, and λ is the cell proliferation constant. The linear quadratic parameters were derived so that the tumor cell loss was represented by an average α of 0.3 Gy^{-1} and α/β of 25 Gy. The cell repair constant was 0.46 h^{-1}. The cell proliferation constant was derived from tumor regrowth data taken for single fraction ^{60}Co experiments for this tumor model. More detail on the calculation method appears in the literature.[13,15]

Comparison Dosimetry

For purposes of comparing dose calculations between studies, it is assumed that the bone marrow is the dose limiting normal organ. The ^{177}Lu radionuclide conjugated to murine CC49 antibody experienced high tumor uptake and low bone uptake.[16] The dose to bone marrow is assumed proportional to the dose to blood,[17] which is dependent on the uptake in blood (Fig. 1a). The ratios of dose to bone marrow for the ^{177}Lu-PA-DOTA-HuCC49 and ^{177}Lu-PA-DOTA-HuCC49ΔCH antibodies are 3.7 and 2.2 for the nonpenetrating only and the penetrating plus nonpenetrating components. The difference in bone marrow response in the mouse is expected to be consistent with the total dose (penetrating plus nonpenetrating). However, in the human, the whole body penetrating/nonpenetrating dose ratio is expected to be lower due to the distance between marrow sites and organs of highest concentration. An intermediate dose to bone marrow ratio of 3 was chosen for the comparison.

RESULTS

Example autoradiographs are shown in Figure 2 for 4 h (panels a and b), 24 h (panels c and d), and 48 h (panels e and f) postinjection for the ^{177}Lu-PA-DOTA-HuCC49ΔCH2 and ^{177}Lu-PA-DOTA-HuCC49 antibodies, respectively. Uptake becomes more uniform with time for both.

The 3D dose calculations use the average uptake as a function of time (Fig. 1b) as input to determine the time course of the tumor activity density per injected dose. The 3D dose-rate in-

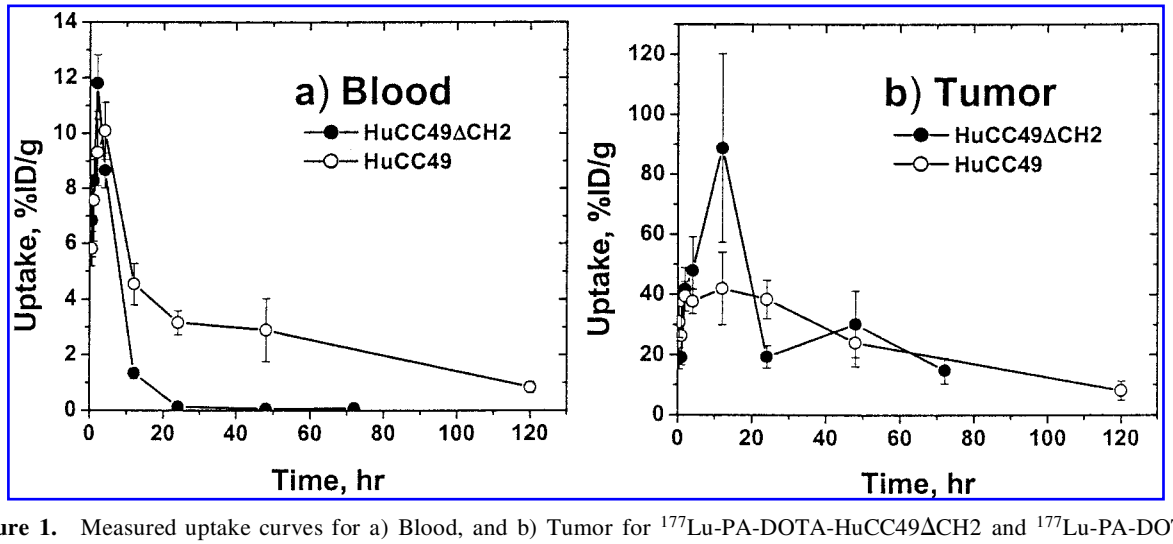

Figure 1. Measured uptake curves for a) Blood, and b) Tumor for ^{177}Lu-PA-DOTA-HuCC49ΔCH2 and ^{177}Lu-PA-DOTA-HuCC49.

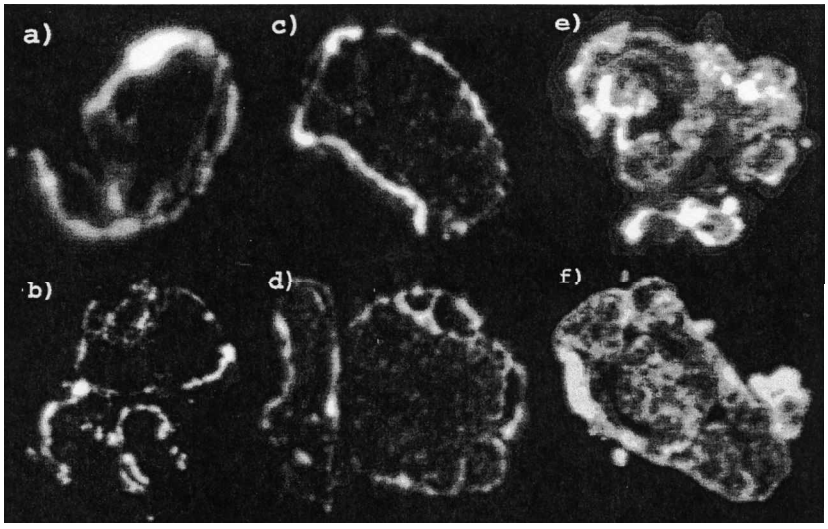

Figure 2. Section images of tumors resected at 4 h (a and b), 24 h (c and d), and 48 h (e and f) postinjection for ^{177}Lu-PA-DOTA-HuCC49ΔCH2 and ^{177}Lu-PA-DOTA-HuCC49, respectively.

formation is contained in the radial histograms, averaged over multiple tumors (histograms appear elsewhere).[9] The numbers of tumors digitally reconstructed at 1 h, 4 h, 24 h, and 48 h postinjection were 5, 6, 8, and 6 for the ^{177}Lu-PA-DOTA-HuCC49ΔCH2 experiments and 3, 5, 9, and 6 for the ^{177}Lu-PA-DOTA-HuCC49 experiments, respectively.

Average radial dose-rate curves derived from the radial histograms illustrate general properties of the time dependence (Fig. 3). They are plotted in cGy/h/μCi to illustrate the change of dose rate over time as a function of radius. At early times, the dose rate peaks at radii near but not at the tumor surface. Central dose rates increase slowly and reach a plateau at later times. The ^{177}Lu-PA-DOTA-HuCC49ΔCH2 antibody retains greater uniformity of dose rate for a longer time. The dose rates at the far surface regions remain lower for both antibodies because surface dose rates are more a function of the isotope's beta spectrum than uptake characteristics. Because of the 3D partial volume increase with radial increment, the dose rate at the largest radial increment represents nearly 10% of the tumor volume.

The uptake curve for ^{177}Lu-PA-DOTA-HuCC49ΔCH2 falls at 24 h, then rises at 48 h. This behavior cannot be attributed solely to nonuniformity of uptake since the average nonuniformity curves (Fig. 3) normalized to the uptake measurements indicate an average increase at all radii. This apparent discrepancy is probably due to statistical fluctuations in the uptake data.

Due to the severe nonuniformity of dose rate, both as a function of radius and range at each radius, the calculation of total dose is not meaningful. Effective dose calculations were performed for a range of injected doses, using the minimum of the fractional cell survival curve. Injected doses were chosen for the ^{177}Lu-PA-DOTA-HuCC49 analysis and three times those values for ^{177}Lu-PA-DOTA-HuCC49ΔCH2. The predicted whole-tumor fractional cell survival reaches a minimum at about 50 h, with the minimum occurring at earlier times for larger injected doses (Fig. 4). General characteristics of lower relative efficacy for higher injected dose is evident by the greater gap between the lower and intermediate injected dose curves compared to the intermediate and higher injected dose curves.

A direct comparison of the two antibodies for the same injected dose illustrates the effect of the difference in uptake patterns (Fig. 5). The difference between curves is due to the difference in uptake and nonuniformity of uptake. All other parameters in the calculation were kept constant. The ^{177}Lu-PA-DOTA-HuCC49ΔCH2 antibody achieves a greater recurrence delay, but a similar curve minimum compared to the ^{177}Lu-PA-DOTA-HuCC49 antibody. The improved uniformity of uptake noted in the radial distributions does not impact the estimated cell survival until after the minimum has been reached.

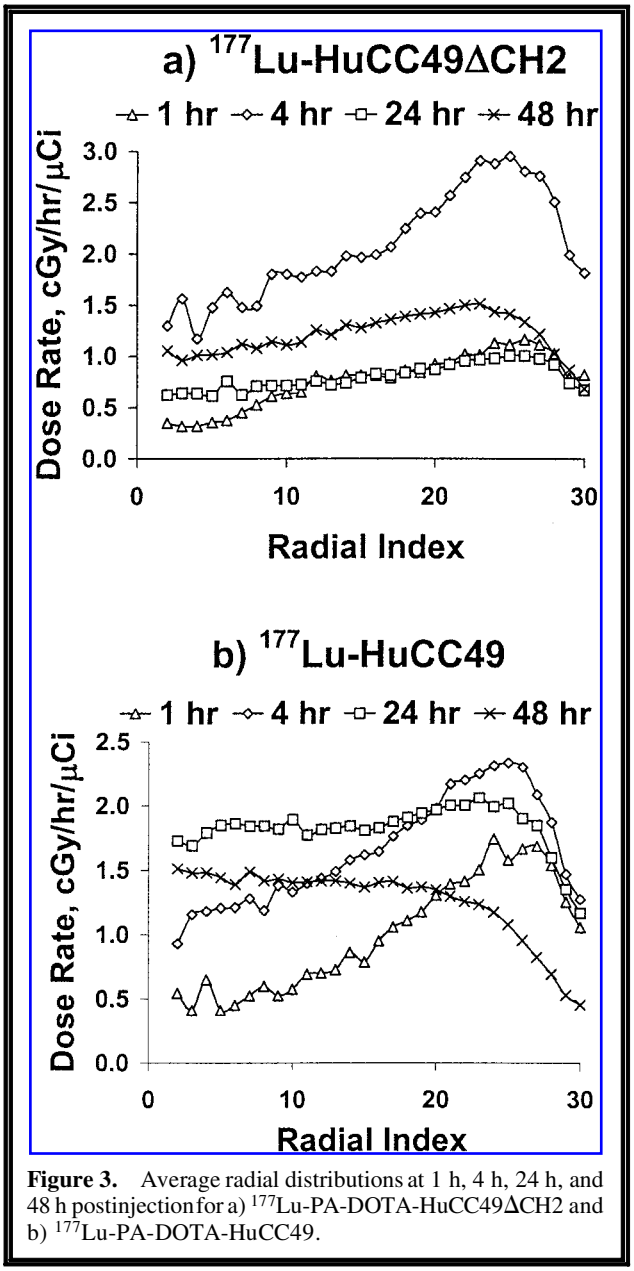

Figure 3. Average radial distributions at 1 h, 4 h, 24 h, and 48 h postinjection for a) ^{177}Lu-PA-DOTA-HuCC49ΔCH2 and b) ^{177}Lu-PA-DOTA-HuCC49.

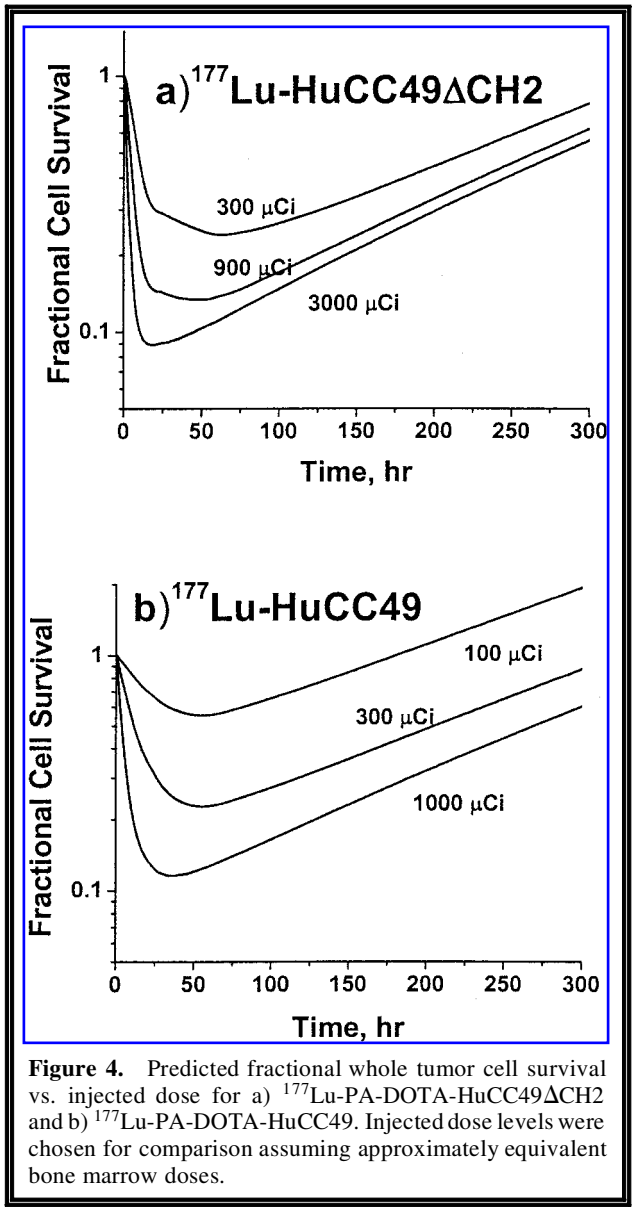

Figure 4. Predicted fractional whole tumor cell survival vs. injected dose for a) ^{177}Lu-PA-DOTA-HuCC49ΔCH2 and b) ^{177}Lu-PA-DOTA-HuCC49. Injected dose levels were chosen for comparison assuming approximately equivalent bone marrow doses.

The estimated fractional cell survival had a considerable radial dependence. Figure 6 shows five sample radii from the surface to near center at regular intervals. At time zero, the fractions of cells are normalized to partial volumes of a sphere. The closer to the tumor surface, the earlier the cell survival minimum and cell number recovery occurs for both antibodies. The corresponding calculations for the lowest injected doses have the surface regions recurring first with the effect getting stronger with increasing injected dose. At later times the fractional volume increases with increasing radius, making this effect dominant.

Estimated effective doses are given in Table 1. Effective dose varies nonlinearly with injected dose due to exponential cell loss with increasing dose and nonuniform uptake and dose rates. These antibodies yield similar results in predicted therapeutic effect, as described by effective dose, for the same injected dose. An effective dose based on time to viable cell recurrence would be more favorable for the ^{177}Lu-PA-DOTA-HuCC49ΔCH2 antibody.

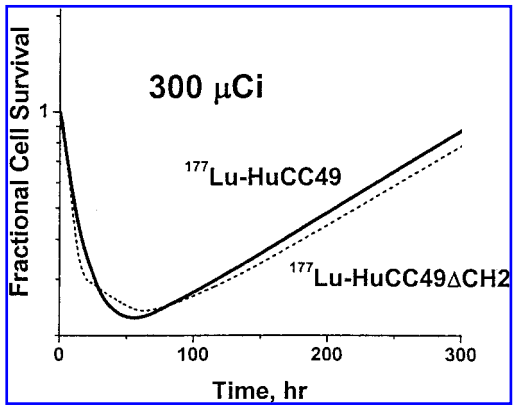

Figure 5. Comparison of fractional cell survival for ^{177}Lu-PA-DOTA-HuCC49ΔCH2 and ^{177}Lu-PA-DOTA-HuCC49 antibodies. An injected dose of 300 μCi is assumed.

DISCUSSION

The nonuniformity of dose and dose rate in tumor is a major concern for radioimmunotherapy. Both the total uptake and nonuniform distribution must be measured to provide a reliable estimate of tumor dosimetry. Since average total dose does not correlate with outcome, a dosimetry model using an effective or equivalent dose definition is justified.

The dosimetry model used here is approximate but useful for comparison of antibody behavior. The difference in magnitude and uniformity of uptake can be described in more useful terms as a difference in predicted minimum cell survival or time to viable cell recurrence. The result from this comparison, that the faster clearance from blood allowing greater injected dose values far outweighs improvement in outcome due to more uniform uptake, is important for the future optimization of radioisotope carriers. However, the improvement in 3D uptake characteristics is also important for optimized therapy.

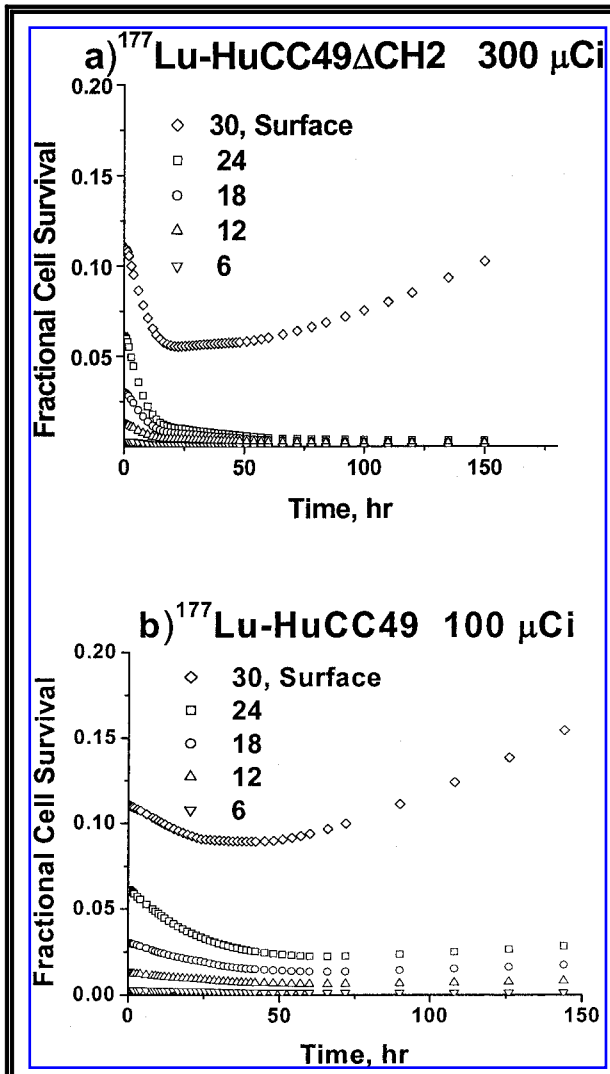

Figure 6. Fractional cell survival for selected radii for a) ^{177}Lu-PA-DOTA-HuCC49ΔCH2 and b) ^{177}Lu-PA-DOTA-HuCC49. The sum for all radii at time zero is unity.

The predicted cell loss curves show a minimum at about 2 days postinjection. This implies that fractionated therapy using about this frequency would yield an improved outcome. If so, the im-

Table 1. Effective Dose and Time to Minimum Cell Survival

^{177}Lu-HuCC49ΔCH2			*^{177}Lu-HuCC49*		
Injected dose, μCi	*Time, hr*	*D_{eff}, Gy*	*Injected dose, μCi*	*Time, hr*	*D_{eff}, Gy*
300	66	4.1	100	57	1.7
900	51	5.7	300	57	4.2
3000	18	6.9	1000	36	6.2

provement in dose uniformity observed for the ^{177}Lu-PA-DOTA-HuCC49ΔCH2 antibody implies that further improvement in outcome could be achieved with additional fractions compared with the ^{177}Lu-PA-DOTA-HuCC49 antibody.

The significant uptake nonuniformity observed in these studies changes with radius, but is present at all radii. The dose rates at the tumor surface are variable, but also systematically lower than more interior dose rates. The lower average dose rate at the tumor surface is predicted to be the weak point in fractional cell loss. As time postinjection increases, the predominantly viable cell population at the well-vascularized surface multiplies more rapidly. The average surface dose rates are always lower than more interior dose rates, and ultimately the surface experiences the lowest average dose rate in the tumor. The combination produces the predicted surface recurrence. Others have observed the dominant effect of surface recurrence in histological studies.[18]

The shortcomings in the tumor model used here include an approximate relationship between necrotic and hypoxic cells and dose rate. The model assumes that there is no correlation between dose rate and cell status. However, since hypoxic cells are more likely to be far from vessels, early uptake is expected to correlate with cell status. At later times, this correlation is expected to decrease because of molecular diffusion and convection producing greater relative uptake uniformity. The model assumes that all of the nonuniformity is due to random tumor architecture. The model also assumes that low-uptake regions stay low-uptake regions. While this assumption sounds reasonable, the greater the injected dose, the greater the outcome depends on the low-uptake regions and thus the more unreliable the model becomes.

The proportion of hypoxic and necrotic regions varies with tumor size and with level of therapy, but is assumed to remain constant in this model. The proportions were set to approximately represent average tumor size. The critical comparison between antibody treatments occurs within 3 days, a time period unlikely to allow a big change in the cell fractions. Extrapolating the present data to therapy levels is of interest, but is expected to be less reliable because the tumor goes through more rapid changes due to early cell loss, probably beyond a couple of cell doubling times (~5 days). This is not expected to impact the minima in the cell loss curves for a bolus injection. The net affect of the proportion and radial dependence of hypoxic and necrotic cells in this model is to increase the importance of cells closer to the tumor surface, which is closer to reality than the assumption of uniform cell composition.

The result that the impact of rapid blood clearance for the smaller molecule is more important than the improvement in nonuniformity of uptake may not be applicable to other tumor-antibody models. If the antibody penetration were very poor for the intact molecule, then the improvement in nonuniformity achieved by the smaller molecule could be more dramatic and possibly dominant. In addition, the improvement in nonuniformity may be more important in larger tumors than presently studied for this tumor-antibody model.

CONCLUSIONS

The comparison of the ^{177}Lu-PA-DOTA-HuCC49ΔCH2 and ^{177}Lu-PA-DOTA-HuCC49 antibodies shows an observable advantage for the HuCC49ΔCH2 antibody in terms of improved dose rate due to more uptake uniformity. However the much larger advantage is the rapid blood clearance, allowing approximately three times the tolerated injected dose, assuming bone marrow as the critical organ. The tumor surface is predicted to be the primary region of recurrence for both antibodies.

ACKNOWLEDGMENTS

The authors thank W.V. Prestwich for performing dose point kernel calculations for the ^{177}Lu isotope, and Sheila Bright, Synethia Kidd, and Christine Olsen for carrying out the antibody studies, and Kristi Schmitt, Erin Lang, and Megan Fitzgerald for data analysis assistance. This work was supported in part by NIH grant CA78505.

REFERENCES

1. Chappell LL, Rogers BE, Khazaeli MB, Mayo MS, Buchsbaum DJ, Brechbiel MW. Improved synthesis of the bifunctional chelating agent 1,4,7,10-tetraaza-*N*-(1-carboxy-3-(4-nitrophenyl)propyl)-*N′*,*N″*,*N‴*-tris(acetic acid)cyclododecane (PA-DOTA). *Bioorg Med Chem* 1999;7:2313–2320.

2. LoBuglio AF, Wheeler RH, Rang J, Haynes AM, Rogers K, Harvey EB, Sun L, Ghrayeb J, Khazaeli MB. Mouse/human chimeric monoclonal antibody in man: Kinetics and immune response. *Proc Natl Acad Sci USA* 1989;86:4220–4224.
3. Meredith RF, LoBuglio AF, Plott WE, Orr RA, Brezovich IA, Russell CD, Harvey EB, Yester MV, Wagner AJ, Spencer SA, Wheeler RH, Saleh MN, Rogers KJ, Polansky A, Salter MM, Khazaeli MB. Pharmacokinetics, immune response, and biodistribution of iodine-131-labeled chimeric mouse/human IgGI, 17-1A monoclonal antibody. *J Nucl Med* 1991;32:1162–1168.
4. Slavin-Chiorini DC, Kashmiri S, Schlom J, Calvo B, Shu LM, Schott ME, Milenic DE, Snoy P, Carrasquillo J, Anderson K, Horan Hand, P. Biological properties of chimeric domain-deleted anticarcinoma immunoglobulins. *Cancer Res (Suppl*) 1995;55:5957s-5967s.
5. Murray JL, Macey DJ, Grant EJ, Rosenblum MG, Kasi LP, Zhang HZ, Kata RL, Rieger PT, LeBherz D, Bhadkamkar VP, South MS, Schlom J, Podoloff DA. Phase II trial of ^{131}I-CC49 Mab plus alpha interferon (rlFNα) in breast cancer. *J Immunother* 1994;16:162.
6. Mulligan T, Carrasquillo JA, Chung Y, Milenic DE, Schlom J, Feuerstein I, Paik C, Perentesis P, Reynolds J, Curt G. Phase I study of intravenous ^{177}Lu-labeled CC49 murine monoclonal antibody in patients with advanced adenocarcinoma. *Clin Cancer Res* 1995;1:1447–1454.
7. Meredith RF, Partridge EE, Alvarez RD, Khazaeli MB, Plott G, Russell CD, Wheeler RH, Liu T, Grizzle WE, Schlom J, LoBuglio AF. Intraperitoneal radioimmunotherapy of ovarian cancer with Lutetium-177-CC49. *J Nucl Med* 1996;37:1491–1496.
8. Howell RW, Rao DV, Sastry KS. Macroscopic dosimetry for radioimmunotherapy: Nonuniform activity distributions in solid tumors. *Med Phys* 1989;16:66–74.
9. Rogers BE, Roberson PL, Shen S, Khazaeli MB, Carpenter M, Yokoyama S, Brechbiel MW, Buchsbaum DJ. Comparison of localization and therapy with ^{177}Lu-PA-DOTA-HuCC49 and ^{177}Lu-PA-DOTA-HuCC49DCH2 in mice bearing intraperitoneal xenografts. Cancer Res, submitted 2003.
10. Prestwich WV, Nunes J, Kwok CS. Beta dose point kernels for radionuclides of potential use in radioimmunotherapy. *J Nucl Med* 1989;30:1036–1046; and 1989;30:1739–1740, and private communication.
11. Roberson PL, Buchsbaum DJ, Heidorn DB, Ten Haken RK. Three-dimensional tumor dosimetry for radioimmunotherapy using serial autoradiography. *Int J Radiat Oncol Biol Phys* 1992;24:329–334.
12. Roberson PL, Heidorn DB, Kessler ML, Ten Haken RK, Buchsbaum DJ. Three-dimensional reconstruction of monoclonal antibody uptake in tumor and calculation of beta dose-rate nonuniformity. *Cancer* 1994;73:912–918.
13. Roberson PL, Buchsbaum DJ. Reconciliation of tumor response to external beam radiotherapy versus radioimmunotherapy with ^{131}Iodine-labeled antibody for a colon cancer model. *Cancer Research (Suppl)* 1995; 55:5811s-5816s.
14. Millar WT. Application of the linear-quadratic model with incomplete repair to radionuclide directed therapy. *Brit J Rad* 1991;64:242–251.
15. Roberson PL, Dudek S, Buchsbaum DJ. Dosimetric comparison of bolus and continuous injections of CC49 monoclonal antibody in a colon cancer xenograft model. *Cancer (Suppl*) 1997;80:2567–2575.
16. Schlom J; Siler K, Milenic DE, Eggensperger D, Colcher D, Miller LS, Houchens D, Cheng R, Kaplan D, Goeckeler W. Monoclonal antibody-based therapy of a human tumor xenograft with a ^{177}lutetium-labeled immunoconjugate. *Cancer Res* 1991;51:2889–2896.
17. Siegel JA, Wessels BW, Watson EE, Stabin MG, Vriesendorp HM, Bradley EW, Badger CC, Brill AB, Kwok CS, Stickney DR, Eckerman KF, Fischer DR, Buchsbaum DJ, Order SE. Bone marrow dosimetry and toxicity for radioimmunotherapy. *Antibody Immunoconj Radiopharm* 1990;3:213–233.
18. Esteban JM, Schlom J, Mornex F, Colcher D. Radioimmunotherapy of athymic mice bearing human colon carcinomas with monoclonal antibody B72.3: Histological and autoradiographic study of effects on tumors and normal organs. *Eur J Cancer Clin Oncol* 1987;23:643–655.

This article has been cited by:

1. Duxin Sun, Mark Bloomston, George Hinkle, Osama Habib Al-Saif, Nathan C. Hall, Stephen P. Povoski, Mark W. Arnold, Edward W. Martin. 2007. Radioimmunoguided surgery (RIGS), PET/CT image-guided surgery, and fluorescence image-guided surgery: Past, present, and future. *Journal of Surgical Oncology* **96**:4, 297-308. [CrossRef]